Vietnam Journal of Science and Technology ***63*** *(6) (2025) 1117-1126*

doi:10.15625/2525-2518/18110

Correlation between electrical properties and critical behavior in $La_{0.7}Ca_{0.25}Ag_{0.05}MnO_3$ nanoparticles

Pham Hong Nam[1, 2], Ta Ngoc Bach[1], Le Viet Bau[3], Nguyen Van Dang[4], Pham Truong Tho[5, 6], Nguyen Xuan Phuc[5, 6], Pham Thanh Phong[5, 6, *]

[1]*Institute of Materials Science, Vietnam Academy of Science and Technology, 18 Hoang Quoc Viet, Nghia Do Ward, Ha Noi, Viet Nam*

[2]*Graduate University of Science and Technology, Vietnam Academy of Science and Technology, 18 Hoang Quoc Viet, Nghia Do Ward, Ha Noi, Viet Nam*

[3]*Hong Duc University, 565 Quang Trung Street,* Hac Thanh Ward, *Thanh Hoa, Viet Nam*

[4]*Department of Physics and Technology, Thai Nguyen University of Science, Phan Dinh Phung Ward, Thai Nguyen, Viet Nam*

[5]*Laboratory of Magnetism and Magnetic Materials, Science and Technology Advanced Institute, Van Lang University, Binh Loi Trung Ward, Ho Chi Minh City, Viet Nam*

[6]*Faculty of Applied Technology, Van Lang School of Technology, Van Lang University, Binh Loi Trung Ward, Ho Chi Minh City, Viet Nam*

[*]Emails: *phamthanhphong@vlu.edu.vn*

Received: 22 February 2023; Accepted for publication: 31 August 2025

Abstract. In this study, we investigated the critical behavior of $La_{0.7}Ca_{0.25}Ag_{0.05}MnO_3$ nanoparticles by analyzing temperature-dependent resistivity data and systematic magnetization measurements performed under an applied magnetic field of 3 T. The critical exponents extracted from the resistivity scaling near the ferromagnetic–paramagnetic transition, $\beta = 0.676$ and $\gamma = 0.734$, closely match those obtained from the Modified Arrott plot method, demonstrating good internal consistency between electrical transport and magnetic characterization approaches. To further assess the reliability and universality of the extracted exponents, the Widom scaling relation was employed, alongside a detailed examination of the magnetization scaling equations. Both analyses confirmed that the critical behavior satisfies the expected scaling constraints over a broad temperature and field range. The convergence of these independent methods provides strong evidence that long-range dipole–dipole interactions play a dominant role in governing the magnetic phase transition of $La_{0.7}Ca_{0.25}Ag_{0.05}MnO_3$ nanoparticles, offering deeper insight into the mechanisms controlling their magnetic and transport properties.

Keywords: nanoparticles, manganites, critical behavior, resistivity.

Classification numbers: 2.4.2, 2.4.4, 5.2.1.

1. INTRODUCTION

In recent years, manganites have attracted considerable attention owing to their intriguing physical phenomena, such as colossal magnetoresistance (CMR) and the magnetocaloric effect

(MCE) [1]. Among these, magnetic refrigeration based on MCE has emerged as a promising alternative to the conventional compression–evaporation cycle for room-temperature applications [2].

Fundamentally, MCE originates from the field-induced magnetic alignment of spins, which reflects the strong spin–lattice coupling in these systems. In manganites, this coupling is further governed by the variation of lattice parameters across the magnetic phase transition [3].

The interplay among magnetism, electronic transport, and charge ordering in doped manganites has been extensively investigated [4]. Nevertheless, most previous studies have primarily focused on the relationship between magnetization and resistivity. The ferromagnetic ordering in such systems is typically characterized by a well-defined set of critical exponents, which to date have been determined by several approaches, including the Modified Arrott plot (MAP), Kouvel–Fisher (KF) analysis, and critical isotherm methods based on magnetization isotherms [5, 6].

Importantly, manganites exhibit a strong correlation between their magnetic and electrical properties, as described by the Fisher–Langer [7] and Suezaki–Mori [8] models. These frameworks have introduced methodologies for extracting critical exponents from resistivity data, an approach that has been increasingly adopted in recent studies [9, 10].

Investigations on nanoscale systems have demonstrated that finite-size and surface effects often dominate over intrinsic bulk characteristics, thereby rendering the synthesis route a decisive factor in determining their physical properties [11, 12]. In particular, the preparation procedure governs the nature of the surface region in nano-sized particles, which plays a pivotal role in shaping their electrical, magnetic, and magneto-transport responses [13]. Although several studies have explored the synthesis of nanophasic manganites via reactive milling-based methods, the correlation between critical exponents and the electrical properties of nanomanganites prepared by this approach remains largely unexplored.

Moreover, analyzing the critical behavior of manganites through resistivity measurements in conjunction with magnetization isotherms offers valuable insights into the influence of magnetic disorder on their transport properties. For this reason, the critical behavior of nanostructured manganites has been comprehensively examined in the present study.

It has been reported that monovalent cations such as Na, K, and Ag can induce ferromagnetism in $LaMnO_3$, with Curie temperatures ranging from 180 to 340 K [14]. Among these, $La_{1-x}Ag_xMnO_3$ is particularly attractive due to its pronounced magnetoresistance (MR) near room temperature [15]. Moreover, $La_{1-x}Ag_xMnO_3$ can stabilize a distorted perovskite manganite structure, owing to the comparable ionic radii of La^{3+} and Ag^{+} [16]. This unique crystal configuration gives rise to remarkable electrical, thermal, and magnetic properties [17], including a significantly enhanced MR at room temperature compared to divalent-doped counterparts [18]. Despite these promising features, studies on the critical behavior of Ag-doped $La_{0.7}Ca_{0.3}MnO_3$ remain scarce.

The electrical transport and magnetoresistive properties of the parent $La_{0.7}Ca_{0.3}MnO_3$ nanoparticles (NPs) have been reported previously [10, 11, 13]. However, the influence of Ag substitution on the critical behavior of Ca-doped manganites remains largely unexplored, particularly in nanoscale systems. Addressing this gap, the present work systematically investigates the critical behavior of $La_{0.7}Ca_{0.25}Ag_{0.05}MnO_3$ (LCAMO) NPs.

Critical exponents were extracted from resistivity measurements using the Fisher–Langer [7] and Suezaki–Mori [8] models, and the results were benchmarked against those obtained from the Modified Arrott plot (MAP) method [5, 6]. The consistency of these approaches not only

validates the reliability of our analysis but also provides new insights into the interplay between magnetic disorder and electronic transport in Ag-doped manganites. This study thus contributes to a deeper understanding of the microscopic mechanisms governing the magneto-transport properties of nanostructured perovskite manganites.

2. MATERIALS AND METHODS

$La_{0.7}Ca_{0.25}Ag_{0.05}MnO_3$ NPs were synthesized via a conventional solid-state reaction method combined with high-energy ball milling. High-purity precursors (99.99%) of La_2O_3, $CaCO_3$, Ag_2O, and MnO were weighed in stoichiometric proportions, thoroughly mixed, and ground. The homogenized mixture was first calcined at 1000 °C for 10 h and subsequently sintered at 1100 °C for another 10 h. The resulting powders were then subjected to high-energy milling for 3 h. Finally, the nanopowders were pressed into pellets under a uniaxial pressure of 10 MPa cm^{-2} and sintered at 900 °C for 5 h.

The structural characteristics and phase purity of the samples were examined using powder X-ray diffraction (XRD) with Cu–Kα_1 radiation (λ = 1.54056 Å). Scanning electron microscopy images (SEM) were recorded using an FE-SEM S4800 equipment. The temperature-dependent resistivity, *R(T)*, of the $La_{0.7}Ca_{0.25}Ag_{0.05}MnO_3$ NPs was measured in the range of 50 - 300 K under applied magnetic fields of 0 and 3 T using a standard four-probe configuration. Isothermal magnetization measurements were performed under fields up to 3 T in the temperature interval of 220 - 280 K employing a Physical Property Measurement System (PPMS, VersaLab model VL173).

3. RESULTS AND DISCUSSION

Figure 1 presents the refined XRD pattern of LCAMO nanoparticles at room temperature. The diffraction data were collected in the 2θ range of 30° - 80° with a scanning rate of 3° min^{-1} and a step size of 0.02°. The nanocrystalline sample is well indexed to an orthorhombic perovskite structure with the *Pnma* space group. The sharp diffraction peaks indicate good crystallinity, and no evidence of secondary phases such as metallic Ag or other impurities was detected, consistent with previous reports on Ag-doped manganites at low doping concentrations ($x \leq 0.15$) [19].

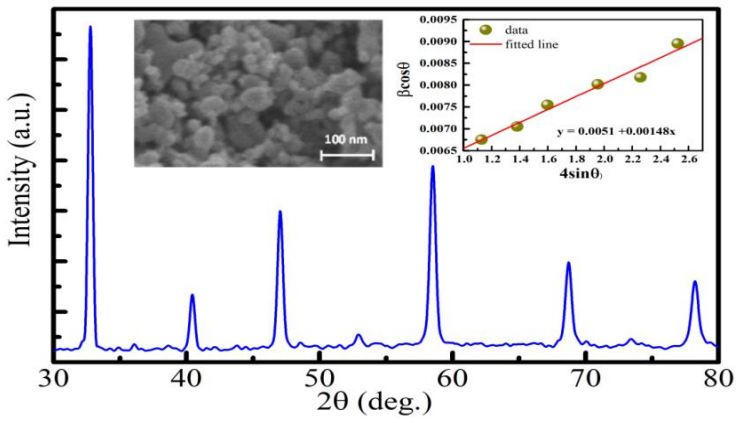

Figure 1. XRD patterns of $La_{0.7}Ca_{0.25}Ag_{0.05}MnO_3$ nanoparticles. The inset shows the W-H plot and SEM micrograph.

The crystallite size (D) and microstrain (ε) were evaluated using the uniform deformation model within the Williamson–Hall (W–H) framework [20]:

$$\beta cos\theta = \frac{k\lambda}{D} + 4\varepsilon sin\theta \quad (1)$$

where β is the full width at half maximum (FWHM) of the selected diffraction peaks, λ is the X-ray wavelength, k (~0.9) is the shape factor, D is the crystallite size, and ε represents the microstrain. Linear regression of the plot of $\beta cos\theta$ versus $4sin\theta$ (inset of Fig. 1) yielded an average crystallite size of 27.18(7) nm and a microstrain of 1.48(1) × 10^{-3}. Complementary SEM analysis revealed a granular morphology with an average particle size of ~35 nm, as shown in the inset of Fig. 1.

Figure 2 shows the temperature dependence of resistivity under applied magnetic fields of 0 and 3 T for LCAMO nanoparticles. The sample exhibits a metal–insulator transition (T_{MI}), defined by the change from metallic behavior $\left(\frac{d\rho}{dT} > 0\right)$ to insulating behavior $\left(\frac{d\rho}{dT} < 0\right)$. Under an applied magnetic field of 3 T, the resistivity peak is suppressed and T_{MI} shifts toward higher temperatures. This effect can be ascribed to the magnetic-field-induced delocalization of charge carriers via spin alignment, which reduces scattering and enhances carrier mobility. Consequently, the paramagnetic semiconducting state is replaced by a ferromagnetic metallic state, characterized by the polarization of conduction electrons $\left(e_g^1\right)$ and an enhanced Mn^{3+} –O–Mn^{4+} double-exchange interaction. As a result, the application of a magnetic field drives T_{MI} to higher temperatures, as illustrated in Fig. 2.

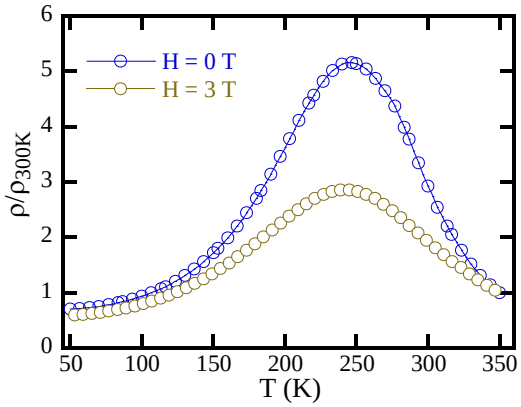

Figure 2. Temperature dependence of the resistivity for LCAMO NPs under magnetic fields of 0 and 3 T.

Magnetic systems undergoing a second-order phase transition are typically classified into universal classes such as three-dimensional (3D) Ising, mean-field, 3D Heisenberg, and tricritical mean-field models. These universality classes are characterized by a set of critical exponents (β, γ, and δ): β describes the spontaneous magnetization below the Curie temperature (T_C), γ characterizes the divergence of the initial susceptibility above T_C, and δ defines the magnetization response at T_C. In practice, these parameters are usually extracted from isothermal magnetization curves using the MAP method, and their validity is confirmed through the Widom scaling relation and scaling equations.

As noted earlier, manganites exhibit a strong correlation between their magnetic and transport properties. Several theoretical models have established a direct link between magnetic phase transitions and electronic conduction mechanisms [7, 8]. This correlation provides a valuable framework for extracting critical exponents from resistivity data. Accordingly, in this

study, we demonstrate that the critical behavior of LCAMO nanoparticles can be effectively evaluated using electrical transport measurements, yielding results consistent with those obtained from conventional magnetization-based methods.

This correlation provides an effective route to identify the critical parameters of manganites through analysis of the resistivity, $R(T)$. Accordingly, our study demonstrates that reliable values of the critical exponents for LCAMO nanoparticles can be extracted from electrical transport measurements. Within the framework of the Fisher–Langer theory [7], the specific-heat exponent (α) is related to the derivative of resistivity with respect to temperature at the metal–insulator transition temperature (T_{MI}):

$$C_p \propto \left(\frac{d\rho}{dT}\right) = \left(\frac{d\rho}{d\eta}\right) = \eta^{-\alpha} \tag{2}$$

where $\eta = [(T - T_{MI})/T_{MI}]$ is the reduced temperature.

This approach was further extended by Geldart *et al.* [21], who formulated two power-law expressions describing the behavior of the specific heat above and below T_{MI}:

$$C(T) = \left[\frac{1}{\rho(T_C)}\frac{d\rho}{dT}\right] = \frac{A^+}{\alpha}[(-\eta)^{-\alpha} - 1] + B^+ \qquad \text{for } T < T_{MI} \tag{3}$$

$$C(T) = \left[\frac{1}{\rho(T_C)}\frac{d\rho}{dT}\right] = \frac{A^-}{\alpha'}\left[(-\eta)^{-\alpha'} - 1\right] + B^- \qquad \text{for } T > T_{MI} \tag{4}$$

where A and B are constants, α and α' denote the critical exponents of the specific heat below and above T_{MI}, respectively.

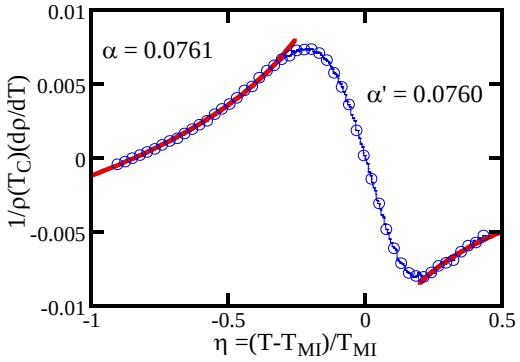

Figure 3. $\left[\frac{1}{\rho(T_C)}\frac{d\rho}{dT}\right]$ as a function of reduced temperature η under an applied magnetic field of 3 T for LCAMO NPs.

Figure 3 shows the variation of $\left[\frac{1}{\rho(T_C)}\frac{d\rho}{dT}\right]$ with reduced temperature $\eta = [(T - T_{MI})/T_{MI}]$. The red solid lines correspond to the best fits of the resistivity data using Eqs. (3) and (4) for temperatures below and above T_{MI}, respectively. The extracted fitting parameters are summarized in Table 1.

Furthermore, the critical exponent γ was evaluated using the Suezaki–Mori model [8], expressed as:

$$\left[\frac{d\rho}{dT}\right] = -\beta_+ \eta^{-(\alpha+\gamma-1)} \quad \text{for } T > T_{MI} \tag{5}$$

which, upon taking the natural logarithm of both sides, yields:

$$ln\frac{d\rho}{dT} = -(\alpha + \gamma - 1)ln\eta + \ln(-\beta_+) \qquad \text{for } T > T_{MI} \tag{6}$$

Here, the slope of the $ln\frac{d\rho}{dT}$ vs. $ln(\eta)$ plot determines the value of $(\alpha + \gamma - 1)$. Since α was previously obtained from the Fisher–Langer analysis, γ can be readily derived. Figure 4 shows the dependence of of $ln\frac{d\rho}{dT}$ on $ln(\eta)$ above T_{MI}, where the slope was found to be −0.190 ± 0.002. Substituting the value of α into Eq. (5), the critical exponent γ was determined as 0.734 ± 0.002.

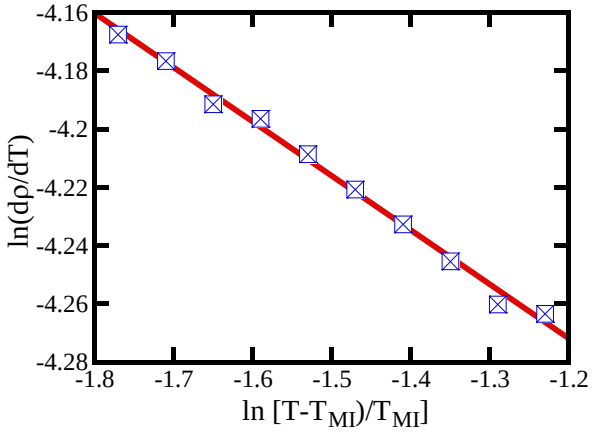

Figure 4. ln $\left(\frac{d\rho}{dT}\right)$ versus ln (η) above T_{MI} under an applied magnetic field of 3 T for LCAMO NPs.

Table 1. Values of different parameters used to fit the experimental data to Eqs. (2) and (3).

Region	*A*	*B*	α	β	γ
$T < T_{MI}$	0.0071 ± 2.31E-05	-0.0012 ± 5.83E-06	0.0761 ± 0.005	-	-
$T > T_{MI}$	-0.0042 ± 0.003	-0.0021 ± 0.0020	0.0761 ± 0.005	0.671 ± 0.002	0.734 ± 0.002

The third critical exponent β was then estimated using the Rushbrooke scaling relation, $\alpha + \gamma + 2\beta = 2$. From this relation, β was obtained as 0.671 ± 0.002.

Interestingly, the extracted critical exponents for LCAMO nanoparticles do not correspond to any of the conventional universality classes. While the 3D Heisenberg model is generally considered consistent with the critical behavior of most manganites [22], the unconventional values observed in this study suggest the presence of long-range dipole–dipole interactions [23].

To further confirm the reliability of the γ and β values derived from electrical transport data, we additionally determined these parameters using the conventional MAP analysis, as presented in the following section.

According to the conventional analysis, the critical exponent β can be extracted from the spontaneous magnetization (M_S) below $T < T_C$ using the relationa

$$M_S(T) = M_0(-\varepsilon)^{\beta} \qquad \text{for } T < T_C \tag{7}$$

whereas γ is related to the inverse initial susceptibility above $T > T_C$ by

$$\chi_0^{-1}(T) = \frac{h_0}{M_0}(-\varepsilon)^{\gamma} \qquad \text{for } T > T_C \tag{8}$$

where $\varepsilon = (T - T_C)/T_C$ denoting the reduced temperature, and M_0 and h_0 being the critical amplitudes.

Figure 5(a) displays the isothermal magnetization curves recorded between 220 and 280 K with a 5 K step across the Curie point. As the applied field increases up to 0.2 T, the magnetization also increases, but no evidence of saturation is observed even at 3 T. To elucidate the nature of the magnetic phase transition**,** Arrott plots (M^2 vs. $(\mu_0 H/M)$) were constructed, as shown in Fig. 5(b). The positive slopes around T_C confirm a second-order ferromagnetic–paramagnetic phase transition in LCAMO nanoparticles [24].

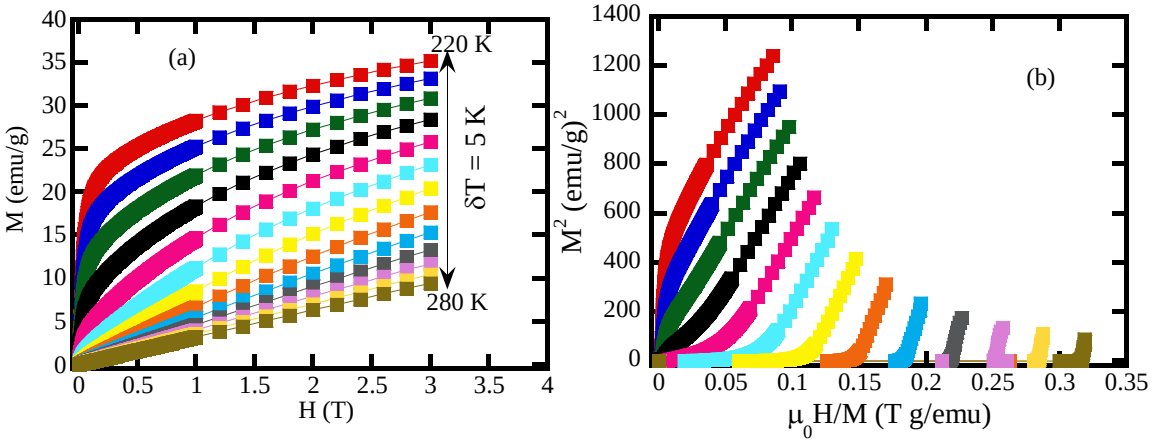

Figure 5. (a) Isothermal magnetization curves measured at different temperatures, and (b) Arrott plots for LCAMO NPs.

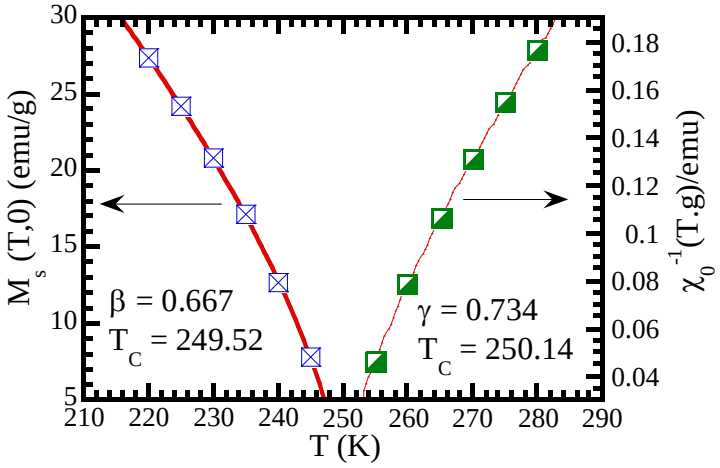

Figure 6. Temperature dependence of both $M_S(T)$ and $\chi_0^{-1}(T)$. The red solid lines present the power-law fits of Eqs. (6) and (7) to $M_S(T)$ and $\chi_0^{-1}(T)$, respectively for LCAMO NPs.

For accurate determination of the critical exponents β and γ from Eqs. (7) and (8), the key step is the reliable estimation of $M_S(T)$ and $\chi_0^{-1}(T)$. In this study, these quantities were obtained from the linear extrapolation of high-field ($\mu_0 H > 2\ T$) Arrott plots, and subsequently analyzed

using a self-consistent fitting procedure [25]. Figure 6 illustrates the temperature dependence of both $M_S(T)$ and $\chi_0^{-1}(T)$, along with the corresponding power-law fits. From these fits, β and γ were determined as 0.667 ± 0.006 and 0.734 ± 0.002, respectively—values that are consistent with those obtained from transport data.

To further assess whether these exponents truly capture the magnetic ordering near T_C, the scaling hypothesis was examined. This hypothesis states that, in the critical regime, the field and magnetization obey the universal scaling form

$$\left(\frac{H}{M}\right)^{1/\gamma} = \frac{T-T_C}{T_1} + \left(\frac{M}{M_1}\right)^{1/\beta} \quad (9)$$

which can be recast as a scaling function of the form $M/|\varepsilon|^{\beta}$ versus $H/|\varepsilon|^{\beta+\gamma}$. As shown in Fig. 7, the data collapse onto two distinct branches corresponding to $T < T_C$ and $T > T_C$, both on linear and logarithmic scales (inset of Fig. 7). This excellent scaling behavior unequivocally validates the critical exponents β and γ, confirming their consistency with the scaling hypothesis for $La_{0.7}Ca_{0.25}Ag_{0.05}MnO_3$ nanoparticles.

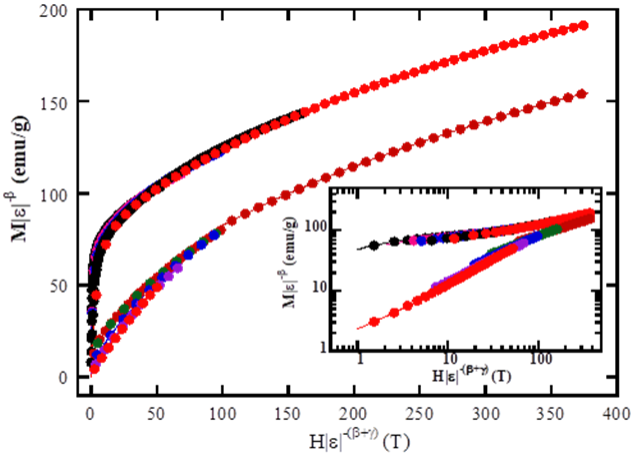

Figure 7. Scale curve specifying the universal aspect one below and above T_c for LCAMO NPs. Insets show the same data for a double logarithmic scale

4. CONCLUSIONS

In this work, the critical behavior of nanocrystallites $La_{0.7}Ca_{0.25}Ag_{0.05}MnO_3$ near the ferromagnetic–paramagnetic transition was systematically investigated by combining magnetic and transport measurements. The extracted critical exponents deviate from those of conventional universality classes, suggesting an unconventional critical regime associated with complex spin interactions. The close consistency between exponents derived from magnetic and electrical analyses highlights the intrinsic coupling between charge transport and magnetic order in this manganite system. Importantly, such non-universal criticality and strong magneto-electric correlations provide new insights into the microscopic mechanisms of phase transitions in doped manganites, which could be exploited for future spintronic and multifunctional device applications.

Acknowledgements. This research is funded by Vietnam National Foundation for Science and Technology Development (NAFOSTED) under grant number 103.02-2019.349.

CRediT authorship contribution statement. Pham Hong Nam: Methodology, Investigation. Ta Ngoc Bach: Formal analysis, Investigation. Le Viet Bau: Formal analysis. Nguyen Van Dang: Formal analysis. Pham Truong Tho: Methodology. Pham Thanh Phong: Investigation, Funding acquisition. Nguyen Xuan Phuc: Supervision,

Declaration of competing interest. The authors declare that they have no known competing financial interests or personal relationships that could have appeared to influence the work reported in this paper.

REFERENCES

1. Yang S. A., Chen Q. M., Hu J., Yang Y. R., Gao Y., Xu R. D., Zhang H., Ma J. - Robust temperature coefficient of resistance of polycrystalline $La_{0.6}Ca_{0.4}MnO_3$ under magnetic fields at room temperature, Ceram. Int. **47** (2021) 29631-29637. https://doi.org/10.1016/j.ceramint.2021.07.132
2. Hemberger J., Brando M., Wehn R., Yu V., Ivanov A., Mukhin A., Balbashov A. M., Loidl A. - Magnetic properties and specific heat of $RMnO_3$ (R = Pr, Nd), Phys. Rev. B **69** (2004) 064418. https://doi.org/10.1103/PhysRevB.69.064418
3. Salamon M. B., Jaime M. - The physics of manganites: structure and transport, Rev. Mod. Phys. **73** (2001) 583-628. https://doi.org/10.1103/RevModPhys.73.583
4. Kouvel J. S. and Fisher M. E. - Detailed Magnetic Behavior of Nickel Near its Curie Point, Phys. Rev. **136** (1964) A1626. https://doi.org/10.1103/PhysRev.136.A1626
5. Fisher M. E., Ma S. K., Nickel B. - Critical Exponents for Long-Range Interactions, Phys. Rev. Lett. 29 (1972) 917. https://doi.org/10.1103/PhysRevLett.29.917
6. Fisher M. E., Langer J. S. - Resistive anomalies at magnetic critical points, Phys. Rev. Lett. **20** (1968)665. https://doi.org/10.1103/PhysRevLett.20.665
7. Suezaki Y., Mori Y. - Dynamic critical phenomena in magnetic systems. II: Electrical resistivity near the Néel point, Prog. Theor. Phys. 41(1969) 1177-1189. https://doi.org/10.1143/PTP.41.1177
8. Khelifi J., Dhahri E., Hlil E. K. - Correlation between electrical, magnetocaloric properties and criticalbehavior in $(La_{0.75}Nd_{0.25})_{2/3}(Ca_{0.8}Sr_{0.2})_{1/3}MnO_3$. Solid State Commun, **249** (2017) 19-23. http://dx.doi.org/10.1016/j.ssc.2016.10.010
9. Mnefgui S., Hassine A. B., Bouazizi M. L., Dhahri A. - Critical Behavior and Its Correlation with Magneto-Electrical Properties in $La_{0.47}Ln_{0.2}Pb_{0.33}MnO_3$ (Ln =Y and Eu) Polycrystalline. J. Low Temp. Phys. 201 (2020) 500-514. https://doi.org/10.1007/s10909-020-02520-4
10. Dey P. and Nath T. K. - Effect of grain size modulation on the magneto- and electronic-transport properties of $La_{0.7}Ca_{0.3}MnO_3$ nanoparticles: The role of spinpolarized tunneling at the enhanced grain surface, Phys. Rev. B **73** (2006) 214425. https://doi.org/10.1103/PhysRevB.73.214425
11. Manh D. H., Phong P. T., Thanh T. D., Nam D. N. H., Hong L. V., Phuc N. X. - Size effects and interactions in $La_{0.7}Ca_{0.3}MnO_3$ nanoparticles, J. Alloys Compd. **509** (2011) 1373-1377. https://doi.org/10.1016/j.jallcom.2010.10.104
12. Navin K., Kurchania R. - The effect of particle size on structural, magnetic and transport properties of $La_{0.7}Sr_{0.3}MnO_3$ nanoparticles, Ceram. Inter. **44** (2018) 4973-4980. Doi: https://doi.org/10.1016/j.ceramint.2017.12.091

13. Manh D. H., Phong P. T., Thanh T. D., Hong L.V., Phuc N. X. - $La_{0.7}Ca_{0.3}MnO_3$ perovskite synthesized by reactive milling method: The effect of particle size on the magnetic and electrical properties, J. Alloys Compd. **491** (2010) 8-12. https://doi.org/10.1016/j.jallcom.2009.10.164
14. Qing X., Li H., Zhong C., Zhou P., Dong Z., Liu J. - Magnetism and spin exchange coupling in strained monolayer CrOCl, Phys. Chem. Chem. Phys. **22** (2020) 17255-17262. https://doi.org/10.1039/D0CP01160F
15. Kar M., Ravi S. - Electrical resistivity and ac susceptibility studies in $La_{1-x}Ag_xMnO_3$. Mater. Sci. Eng. B **110** (2004) 46-51. https://doi.org/10.1016/j.mseb.2004.02.009
16. Xia W., Leng K., Tang Q., Yang L., Xie Y., Wu Z., Zhu X. - Comparative studies on the structural, magnetic, and optical propertiesof perovskite $Ln_{0.67}Ca_{0.33}MnO_3$ (Ln = La, Pr, Nd, and Sm) manganite nanoparticles synthesized by sol-gel method, AIP Advances **11** (2021) 035007. https://doi.org/10.1063/5.0036723
17. Boora N., Ahmad R., Rani P., Maheshwari P. K., Khosla A., Bansal S., Awana V. P. S., Hafiz A. K. - Room Temperature Synthesis of Colossal Magneto-Resistance of $La_{2/3}Ca_{1/3}MnO_3$: $Ag_{0.10}$ Composite, ECS J. Solid State Sci. Tech. **10** (2021) 027006. https://doi.org/10.1149/2162-8777/abe58d
18. Battabyal M., Dey T. K. - Solid State Commun. **134** (2005) 837. https://doi.org/10.1016/j.ssc.2005.01.023
19. Pi L., Hervieu M., Maignan A., Martin C., Raveau B. - Structural and magnetic phase diagram and room temperature CMR effect of $La_{1-x}Ag_xMnO_3$, Solid State Commun. **126** (2003) 229. Doi: https://doi.org/10.1016/S0038-1098(02)00890-6
20. Williamson G. K., Hall W. H. - X-ray line broadening from filed aluminum and wolfram. Acta Metall. **1** (1953) 22. https://doi.org/10.1016/0001-6160(53)90006-6
21. Geldart D. J. W. and Richard T. G. - Theory of spin-fluctuation resistivity near the critical point of ferromagnets, Phys. Rev. B **12** (1975) 5175. https://doi.org/10.1103/PhysRevB.12.5175
22. Skini R., Baaziz H., Tozri A., Abdel-Hafez M., Hassan A. - Magnetocaloric effect and critical behavior in $La_{0.8}K_{0.2}MnO_3$ nanoparticle, Results in Physics **30** (2021) 104861. Doi: https://doi.org/10.1016/j.rinp.2021.104861
23. Tozri A., Dhahri E., Hlil E. K. - Impact of vacancy and Na substitutions on the critical magnetic behavior in polycrystalline $La_{0.8}Pb_{0.2}MnO_3$, Phys. Lett. A **375** (2011) 1528-1533. https://doi.org/10.1016/j.physleta.2011.02.038
24. Arrott A., Noakes J.E. - Approximate Equation of State For Nickel Near its Critical Temperature, Phys. Rev. Lett. **19** (1967) 786-789. https://doi.org/10.1103/PhysRevLett.19.786
25. Stanley H. E. - Scaling, universality, and renormalization: Three pillars of modern critical phenomena, Rev. Mod. Phys. **71** (1999) S358. https://doi.org/10.1103/RevModPhys.71.S358